ACS OMEGA

http://pubs.acs.org/journal/acsodf

Article

Heat-Induced Dry Hydrolysis of Sodium Borohydride/Oxalic Acid Dihydrate Composite for Hydrogen Production

Seunghun Shin, Yunkyeong Kim, Joon-Hyung Jin,* and Jihoon Jung*

Cite This: *ACS Omega* 2022, 7, 979−986

Read Online

ACCESS | Metrics & More | Article Recommendations | Supporting Information

ABSTRACT: The generation of hydrogen, free of poisonous gas, combined with a lightweight proton-exchange membrane fuel cell can expand the use of hydrogen energy from conventional ground transportation vehicles and power stations to a variety of flying vehicles and wearable devices for civilian and military purposes. Herein, a hydrogen fuel composite composed of sodium borohydride (SB) and oxalic acid dihydrate ($OA{\cdot}2H_2O$) is introduced. The $SB/OA{\cdot}2H_2O$ composite was easily decomposed to generate pure hydrogen at a trigger temperature of 50 °C, at which the water molecules of the $OA{\cdot}2H_2O$ component were effectively liberated, inducing hydrolysis of the SB component to produce hydrogen gas. This dry hydrolysis-based hydrogen generation using the $SB/OA{\cdot}2H_2O$ composite has the merits of rapidly generating hydrogen (i.e., 0.4 g of the composite can be fully decomposed within a minute at low temperatures), free of poisonous gas, in approximately 5 wt % yield (the theoretical maximum value).

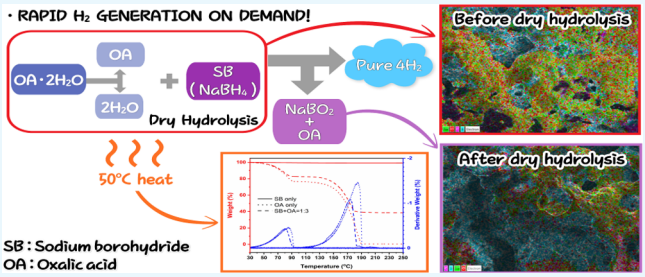

INTRODUCTION

Recent climate change, mostly due to the widespread use of fossil fuels that inevitably generate enormous amounts of greenhouse gases each year, has shifted the focus of researchers and engineers to constructing new power supplies that utilize zero-carbon energy sources such as geothermal, solar power, and wind power.[1−7] Hydrogen, a zero-carbon fuel, has been investigated for decades because the specific energy density of hydrogen is roughly 3 times that of gasoline, that is, 120 MJ kg^{-1} for hydrogen and 44 MJ kg^{-1} for gasoline.[8,9] As a clean energy source, hydrogen can liberate huge amounts of energy via the oxidative reaction with pure oxygen, while negligible amounts of unwanted byproducts are produced by the reaction.[10−14]

However, the mass production of hydrogen via traditional steam reforming of hydrocarbons or water electrolysis is commercially unfavorable and is not environmentally friendly.[15−19] Most importantly, safe storage and transport of the highly explosive hydrogen gas must be ensured for commercial use of hydrogen sources.[10,20−22] More importantly, the operation of proton exchange membrane fuel cell (PEMFC)-driven flying vehicles or portable appliances requires a much lighter hydrogen container with a higher hydrogen volume density than the traditional gas container, which is designed to store extremely compressed or even liquefied hydrogen.[23−26] In contrast, chemical storage as an alternative to the old-fashioned physical storage method is lightweight and has excellent stability under normal conditions.[27,28] Sodium borohydride (SB) is an example of a material for the chemical storage of hydrogen energy and contains 10.6 wt % hydrogen.[29] SB can be cleaved by both hydrolysis and thermolysis to produce pure hydrogen gas.[25] Practically, carbon- and nitrogen-free SB is chemically stable, of low cost, and does not generate gas-phase contaminants such as CO and NH_3 during decomposition, which are recognized as being poisonous to fuel cells.[30,31]

The thermal decomposition[32−35] and the hydrolytic decomposition[36−38] reactions of SB can be described by eqs 1 and 2, respectively.

$$\text{Thermolysis: } NaBH_4 \rightarrow Na + B + 2H_2\uparrow \quad (1)$$

$$\text{Hydrolysis: } NaBH_4 + 2H_2O \rightarrow NaBO_2 + 4H_2\uparrow \quad (2)$$

SB undergoes thermal decomposition at ∼500 °C, where this temperature is incompatible with the normal operating conditions of the PEMFC,[39] while the hydrolytic decomposition of SB suffers from poor control of the reaction speed and safety problems even though it occurs at a reasonable temperature. Frankly, the US Department of Energy declared the hydrolysis of SB to be unsafe for commercial hydrogen generation in 2007.[40]

Received: October 6, 2021
Accepted: December 14, 2021
Published: December 28, 2021

In this study, a new approach for the dehydrogenation of SB is presented, that is, a solid-phase composite of SB and a hydrate compound are prepared. Dehydration of the composite by heating liberates water, which hydrolytically decomposes SB to produce hydrogen (patent pending in KIPRIS, application number 10-2020-0110842). The prepared SB/oxalic acid dihydrate ($OA{\cdot}2H_2O$) is stored in the solid state and is stable under normal conditions. The composite can generate hydrogen on demand with only a small amount of heat to trigger the exothermic dehydrogenation reaction. A previous study verified that $OA{\cdot}2H_2O$ is the best counter compound for SB with an adequate dehydration temperature and molecular mass.[41] Even though studies on the hydrolysis of the $SB/OA{\cdot}2H_2O$ composite have been introduced,[41,42] some challenging issues such as the weight gain caused by the use of the solvent and the poor solubility of $NaBO_2$ in water still remain unresolved.[42] The heat-induced dry hydrolysis of the $SB/OA{\cdot}2H_2O$ composite demonstrated herein does not use any solvent but does use thermally dehydrated water molecules to hydrolyze the composite and eventually produces pure hydrogen from the composite. The composition and reaction conditions of the composite are carefully optimized by characterizing the physicochemical properties of the composite before and after thermo-hydrolytic decomposition.

EXPERIMENTAL METHODS

Reagents and Materials. The substances used to prepare the composite were SB ($NaBH_4$, Sigma-Aldrich, ≥98%, USA) and OA dihydrate [$(COOH)_2{\cdot}2H_2O$, Kanto Chemical, 99.5−102%, Japan], which were sufficiently ground before use. The representative weight ratios of SB in the $SB/OA{\cdot}2H_2O$ composite were 50, 33.3, and 25 wt %. Each mixture was placed in a vial and stirred well using a mechanical mixer (Voltex Genie2 Mixer, Scientific Industries, Inc.).

Laboratory-Designed Reactor for Dry Hydrolysis. The hydrogen generation reactor used in this study is schematically illustrated in Figure S1. The hydrogen generator consists of a digital pressure gauge (0−700 kPa), a heating jacket, and a control box containing a personal computer (PC) and three thermocouples. The actual volume of the inner space of the reactor was 44.6 mL. Two thermocouples were used for feedback control of the reactor temperature, and the third thermocouple was placed inside the vial containing the $SB/OA{\cdot}2H_2O$ composite to determine the temperature inside the vial. After placing the vial in the reactor, the reactor was purged with Ar gas. The inner temperature of the reactor was then raised to the desired temperature at a fixed heating rate and maintained for 30 min at the set temperature. Changes in temperature and pressure inside the reactor were recorded in real time by the reactor control box that was interfaced with a PC.

Equipment. The composition of the gaseous products generated by the reaction was analyzed using gas chromatography and mass spectrometry (GC/MS) (5977E Agilent) with a thermal conductivity detector (TCD) (6890N, Agilent). An Agilent HP-5MS column with a diameter of 250 μm was used for the analyses, along with a 0.25 μm thick film. Thermogravimetric analysis (TGA) (SDT Q600, TA Instruments) was performed to determine the reaction temperature of the $SB/OA{\cdot}2H_2O$ composite. Scanning electron microscopy (SEM), energy dispersive X-ray spectroscopy (EDS) (JSM-7610F, JEOL), and Fourier transform infrared spectroscopy (FTIR) (ALPHA, Bruker) were performed to determine the physicochemical properties of the mixture before and after the decomposition reaction.

Mechanism of Dry-Hydrolytic Decomposition of the $SB/OA{\cdot}2H_2O$ Composite. Figure 1 illustrates the suggested mechanism of decomposition of the $SB/OA{\cdot}2H_2O$ composite by dry hydrolysis. According to eq 2, the composite containing equal amounts of SB and $OA{\cdot}2H_2O$ can generate pure hydrogen with a theoretical maximum H_2 yield of 4.92 wt %, where an important assumption is that the $SB/OA{\cdot}2H_2O$ composite undergoes dry-hydrolytic decomposition without producing any harmful gases (such as carbon oxides) that are incompatible with typical PEMFCs under the given pressure and temperature conditions. OA and $NaBO_2$ are chemically and physically stable at temperatures lower than 100 °C.

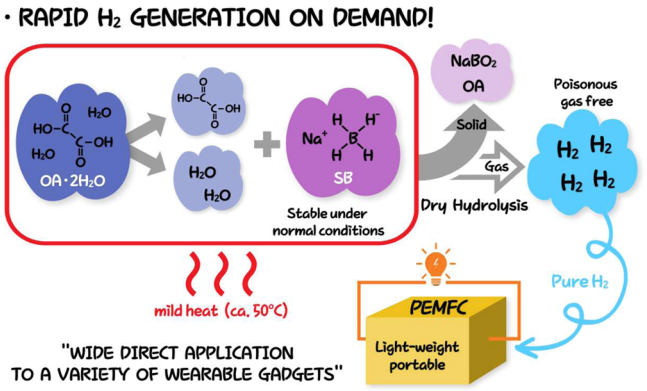

Figure 1. Illustration of the mechanism of decomposition of the $SB/OA{\cdot}2H_2O$ composite by dry hydrolysis. It is assumed that the composite is fully decomposed by the dry hydrolysis without notable production of poisonous contaminants under the given experimental conditions.

RESULTS AND DISCUSSION

Characterization of Dry Hydrolysis of the $SB/OA{\cdot}2H_2O$ Composite. The reaction conditions (weight ratio of SB in the composite and heating rate) for the dry hydrolysis were characterized and optimized. The final temperature of the reactor was set to maximize the hydrogen production. Figure 2a shows the real-time change in the inner pressure of the reactor during dry hydrolysis of the composites. Figure 2b shows the variation of the working temperature of the system when the reactor was heated at a rate of 2 °C min^{-1}. After preheating the reactor to the initial set point of 30 °C for 5 min, the reactor temperature was increased to 50 °C at a rate of 2 °C min^{-1} and was maintained until the end of the reaction. An abrupt increase in the reactor temperature owing to the highly exothermic hydrogen evolution reaction was observed at 48−50 °C, and the dry hydrolysis of each composite was completed within 1 min. These results show that the $SB/OA{\cdot}2H_2O$ composite, which is stable under normal atmospheric conditions, can be effectively decomposed to produce pure hydrogen on demand with only a small triggering temperature. The hydrogen yield determined from eq 3 increased slightly from 4.85 to 5.00 wt % as the OA component in the composite increased from 50 to 75 wt %. The hydrogen yield of 5.00 wt % at a temperature of 50 °C is a better result than a previous result which was obtained by the use of SB and boric acid.[43] The detailed calculation for determining the hydrogen yield is as follows

https://doi.org/10.1021/acsomega.1c05571
ACS Omega 2022, 7, 979−986

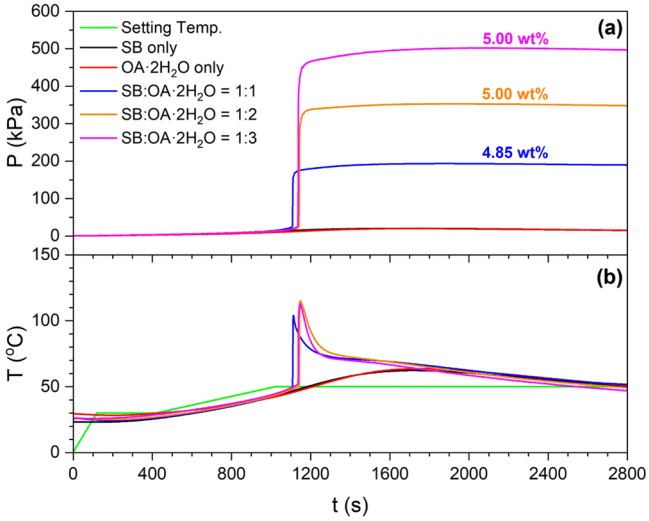

Figure 2. (a) Pressure and (b) temperature changes of the reactor upon dry hydrolysis of SB/OA·2H_2O composites at a heating rate of 2 °C min^{-1}. Note that the green solid line represents the set temperature profile.

$$H_2 \text{ yield (wt \%)} = \frac{\text{weight of the produced } H_2 \text{ (g)}}{\text{total weight of reactants (g)}} \times 100 \quad (3)$$

where the exact volume of the produced hydrogen gas (mL) is equal to the final pressure of the reactor (in absolute pressure) multiplied by the reactor volume (44.6 mL) divided by 101.325 kPa, which is further converted into the weight of hydrogen by multiplying by the hydrogen density at the final temperature of the reactor, for example, 75.1 μg mL^{-1} at 50 °C, 65.3 μg mL^{-1} at 100 °C, and 57.8 μg mL^{-1} at 150 °C.

Neither SB nor OA can generate hydrogen gas individually, even though they both contain hydrogen. This result was verified by the lack of a pressure increase or an abrupt temperature increase with the individual components.

Figure 3 shows the dependence of the hydrogen yield on the heating rate of the SB/OA·2H_2O composite containing 75 wt % OA·2H_2O (SB/OA·2H_2O = 1:3). The total weight of the composite was 0.4 g, and the heating rate was varied as 1, 2, 5, and 10 °C min^{-1}. The pressure curve shown in Figure 3a shows a decline in the total volume of the produced hydrogen gas to 4.78 wt % when the heating rate was reduced to 1 °C min^{-1}. The hydrogen yield increased from 4.78 to 5.10 wt % as the heating rate increased from 1 to 5 °C min^{-1}, and the yield was essentially saturated at 5.10 wt % until the heating rate reached 10 °C min^{-1}. The onset temperature of the dehydrogenation reaction increased to 57.9 °C when the reactor was heated at a rate of 1 °C min^{-1} and decreased to 50.6 °C at 2 °C min^{-1} and to 48.7 °C at 5 °C min^{-1}, as shown in Figure 3b. At a heating rate of 10 °C min^{-1}, the onset temperature increased to 51.8 °C. Note that the onset time decreased as the heating rate increased. This result indicates that the faster the heating rate of the reactor, the faster the hydrogen generation. However, it is difficult to control the feedback of the reactor temperature and suppress unwanted gas evolution because of the temperature overshoot in the reactor at a high heating speed.

Figure 4a,b shows the pressure and temperature changes of the reactor during dry hydrolysis of the SB/OA·2H_2O composite depending on the final set temperature of the

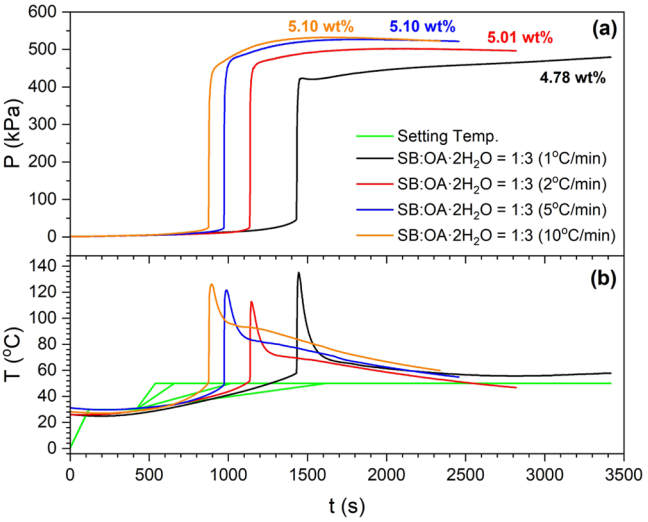

Figure 3. (a) Pressure and (b) temperature changes of the reactor upon dry hydrolysis of the SB/OA·2H_2O composite containing 75 wt % OA·2H_2O (SB/OA·2H_2O = 1:3) at various heating rates, i.e., 1, 2, 5, and 10 °C min^{-1}.

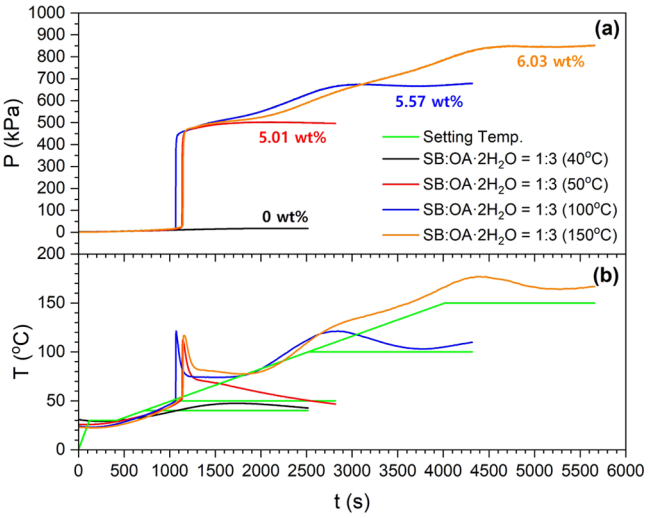

Figure 4. (a) Pressure and (b) temperature changes of the reactor upon dry hydrolysis of the SB/OA·2H_2O composite containing 75 wt % OA·2H_2O (SB/OA·2H_2O = 1:3) at various set temperatures of the reactor, i.e., 40, 50, 100, and 150 °C. Note that no pressure or temperature increase was observed at 40 °C.

reactor. The composite (0.4 g) contains 75 wt % OA·2H_2O (SB/OA·2H_2O = 1:3); the final temperature of the reactor was set to 40, 50, 100, and 150 °C and was achieved by a heating rate of 2 °C min^{-1}. Because a large heat fluctuation occurred at this high rate owing to feedback control lag between the heater and the thermocouple of the reactor, the heating rate was intentionally slowed to 2 °C min^{-1} for better feedback control of the reactor temperature and effective suppression of unwanted gas evolution. Overall, the hydrogen yield increased as the set temperature of the reactor increased, that is, 5.01 wt % at 50 °C, 5.57 wt % at 100 °C, and 6.03 wt % at 150 °C. The hydrogen yield was higher than the theoretical maximum of 4.92 wt %, plausibly due to gaseous contaminants, including carbon monoxide and carbon dioxide, produced by the thermal decomposition of OA at temperatures higher than 100 °C (see Figure S3b). Note that dry hydrolysis of the SB/OA·2H_2O

https://doi.org/10.1021/acsomega.1c05571
ACS Omega 2022, 7, 979−986

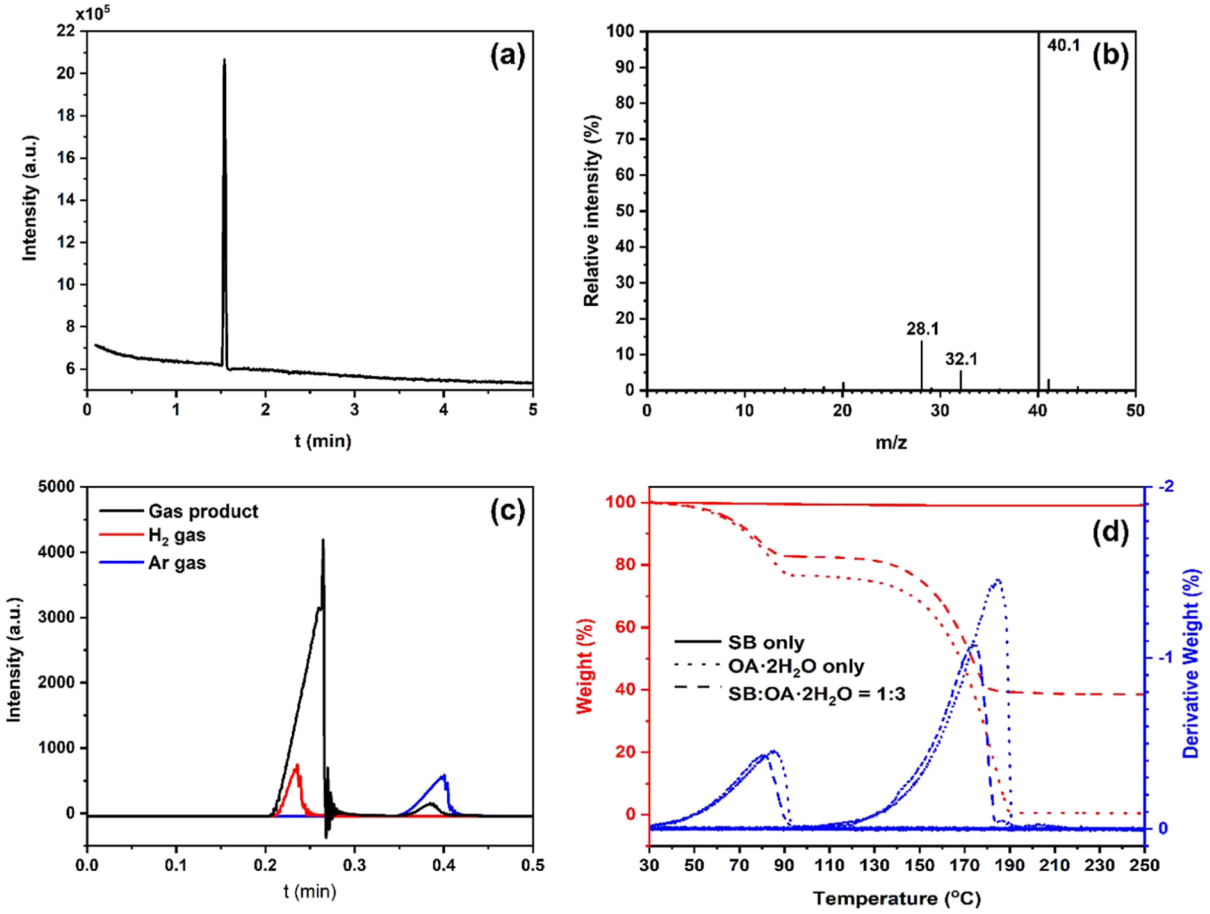

Figure 5. GC (a) and MS (b) spectra of gaseous products obtained from decomposition of the SB/OA·2H_2O composite containing 75 wt % OA·2H_2O (SB/OA·2H_2O = 1:3) via dry hydrolysis. Note that the heating rate and the set temperature of the reactor are 2 °C min^{-1} and 100 °C, respectively. (c) Gas chromatogram of the TCD response to the pyrolytic hydrogen generation via dry hydrolysis of the SB/OA·2H_2O composite. The responses to 10% H_2 (red line) and pure Ar gas (blue line) are also shown for comparison. (d) TGA diagrams of pure SB, pure OA·2H_2O, and the SB/OA·2H_2O composite (SB/OA·2H_2O = 1:3).

composite did not proceed at 40 °C, as verified by the lack of a pressure or temperature increase at the final set temperature of 40 °C.

Characterization of Gaseous Products Generated by Dry Hydrolysis. The gaseous products of the dry-hydrolyzed SB/OA·2H_2O composite, excluding hydrogen gas, were identified by collecting the generated gases using a gas sampling bag (Tedlar Bag, 1 L vol, Supelco) and subsequently injecting 2 μL of this gas sample into the GC−MS instrument. The resulting GC diagram in Figure 5a shows a sharp single peak at a retention time (t_R) of 1.545 min. The corresponding MS spectrum shown in Figure 5b indicates the absence of the molecular ion peaks at m/z = 37.8 SB and m/z = 90.0, assigned to anhydrous OA, and at m/z = 126.1 for OA·2H_2O. Instead, Ar (m/z = 40) used as the purging gas gave rise to a base peak with a small amount of air contaminants, that is, m/z = 28.1 for N_2 and m/z = 32.1 for O_2, indicating that the dry hydrolysis of the SB/OA·2H_2O composite can generate pure hydrogen without producing any harmful gases that are incompatible with the conventional operation of PEMFCs. Note that the GC diagram and the MS spectrum of the air are presented for comparison in Figure S2a,b, respectively. The single peak shown at t_R = 1.545 min owing to the flow of the air is either commonly observed in SB/OA·2H_2O or the air undergoes dry hydrolysis. The peaks assigned to the three most abundant gases in the atmosphere, that is, N_2 (m/z = 28.1), O_2 (m/z = 32.1), and Ar (m/z = 40.1) peaks are clearly observed with small percentages of N (m/z = 14), O (m/z = 16), and H_2O (m/z = 18).[44]

Figure 5c displays the TCD response to the gaseous products generated by the dry hydrolysis of the SB/OA·2H_2O composite. The TCD response to hydrogen gas was calibrated with 5, 10, and 30% hydrogen references, and the results showed that the gas products obtained by the dry hydrolytic dehydrogenation of the composite contained mostly pure hydrogen and a small portion of Ar gas without harmful gases that can potentially poison the PEMFC. The TGA profiles of SB, OA·2H_2O, and the SB/OA·2H_2O composite shown in Figure 5d indicate that SB is chemically stable at temperatures up to 250 °C, and no weight loss was observed. Note that conventionally, a temperature of 500 °C is required for thermal decomposition of SB to produce hydrogen.[32,39,45,46] The weight of OA·2H_2O starts to decrease at approximately 50 °C, and eventually, the weight is saturated at a weight loss of 28%, which corresponds exactly to the weight ratio of H_2O in OA·2H_2O. The weight loss of the SB/OA·2H_2O composite also starts at 50 °C, meaning that the water molecules liberated from the OA·2H_2O component in the composite initiate hydrolytic dehydrogenation of the composite, with simultaneous generation of hydrogen. The saturation of the weight

https://doi.org/10.1021/acsomega.1c05571
ACS Omega 2022, 7, 979−986

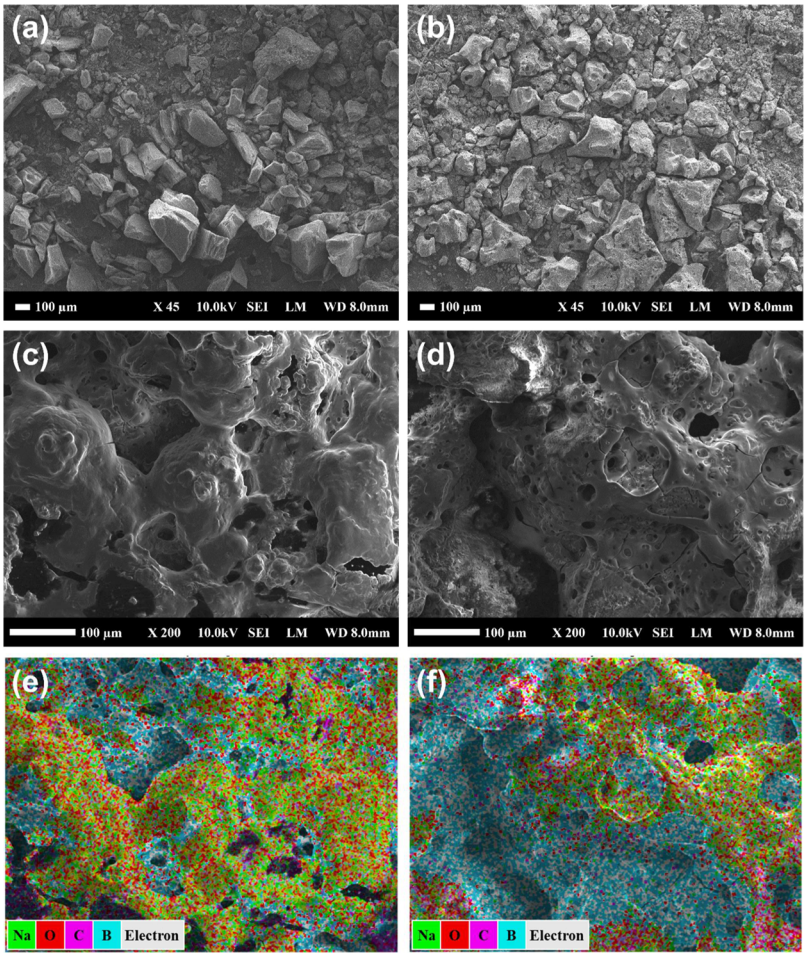

Figure 6. SEM images of the SB/OA·2H_2O composite before (a,c) and after (b,d) dry hydrolysis, at different magnifications. Corresponding EDS mapping images before (e) and after (f) dry hydrolytic dehydrogenation of the composite.

loss of the composite at 40 wt % further verifies that the remainder of the dry hydrolytically decomposed OA·2H_2O is sodium metaborate. Note that OA starts to decompose further into water, carbon monoxide, and carbon dioxide around 110 °C, and no solid product remained above 190 °C. The resulting GC profile of the gaseous product from OA·2H_2O decomposition at 150 °C shows a sharp single peak at t_R = 1.539 min, and the corresponding MS spectrum clearly shows a shift in the base peak from m/z = 40.1 (Ar purging gas) to m/z = 44.1 (CO_2 from the decomposition of OA) (Figure S3a,b). In addition, a large increase in the intensity ratio of the peak at m/z = 28.1 to the peak at m/z = 32 was observed, presumably because CO gas generated from the decomposition of OA strongly increases the intensity of the peak at m/z = 28.1. Even though decomposition of the SB/OA·2H_2O composite at 150 °C resulted in a sharp single peak at t_R = 1.489 min in the GC diagram, the Ar gas used for purging gives rise to a base peak, with a small CO_2 peak in the MS spectrum (Figure S3c,d).

Microscopic Characterization of the SB/OA·2H_2O Composite before and after Dry Hydrolysis. SEM images of the SB/OA·2H_2O composite containing 75 wt % OA·2H_2O (SB/OA·2H_2O = 1:3) before and after the dry hydrolytic dehydrogenation reaction indicated that the particles of the composite became rounded with numerous tiny holes and cracks, whereas angular granules constituted the as-prepared SB/OA·2H_2O composite (Figure 6a,b). The holes and cracks clearly observed in the magnified SEM images in Figure 6c,d are probably due to the fast evolution of heat and H_2 gas generation during the exothermic dehydrogenation reaction. The elemental mapping images obtained from the EDS profiles of the composite before and after the reaction are presented in Figure 6e,f, respectively. The atomic percentages obtained from mapping each element, that is, green for sodium, cyan for boron, pink for carbon, and red for oxygen, are summarized in Table 1. The ratios of the atomic % of B, C, and O to that of Na were 2.51, 1.20, and 3.16, respectively, after the dry hydrolysis, while the corresponding ratios were 2.36, 0.84, and 2.36 before the reaction. As a result, the C/Na and O/Na ratios increased significantly after the reaction, with a small increase in B/Na. Accordingly, it is reasonable to say that a

Table 1. Elemental Coverage in Atomic % of the SB/OA·2H_2O Composite before and after Dry Hydrolytic Dehydrogenation

element	before reaction (atomic %)	after reaction (atomic %)
B (cyan)	35.96	31.90
C (pink)	12.77	15.23
O (red)	36.02	40.16
Na (green)	15.25	12.71
total	100.00	100.00

https://doi.org/10.1021/acsomega.1c05571
ACS Omega 2022, 7, 979−986

large amount of hydrogen gas was generated by the reaction because there were no remaining elements except hydrogen.

Spectroscopic Characterization of the SB/OA·2H_2O Composite before and after Dry Hydrolysis. As shown in Figure S4a, the FTIR spectra of SB before and after dry hydrolysis both show multiple peaks around 2250 cm^{-1} and a strong single peak at 1100 cm^{-1}, assigned to B−H stretching and bending vibrations, respectively. Other multiple peaks at 3000−3500 cm^{-1} were assigned to the O−H stretching vibration, and those at 1250−1500 cm^{-1} were assigned to the B−O stretching vibration which presumably originated from nonspecifically adsorbed water molecules.[47−49] Figure S4b displays the FTIR spectra of OA·2H_2O, showing a broad O−H stretching vibration at 3250−3500 cm^{-1}, carboxylic acid conjugated C═O stretching around 1700 cm^{-1}, O−H bending at 1250 cm^{-1}, and C−O stretching vibration at 1100 cm^{-1}.[50] The SB-specific and OA-specific peaks did not change before and after the dry hydrolytic dehydrogenation of each compound, indicating that both SB and OA would be inactive in the dry hydrolytic process when used individually. The broad strong peak of the SB/OA·2H_2O composite at 3500 cm^{-1}, assigned to the O−H stretching vibration, was downshifted to 3200 cm^{-1} after dry hydrolysis; the peak was also weakened owing to the loss of hydrogen bonds (Figure 7).

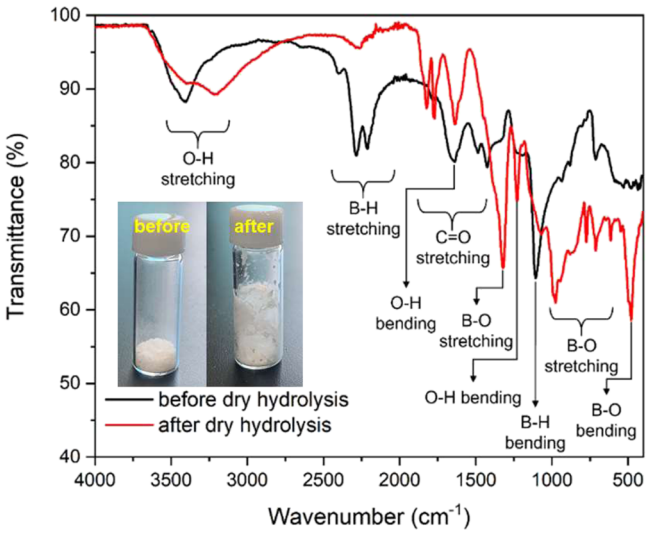

Figure 7. FTIR spectra of the SB/OA·2H_2O composite containing 75 wt % OA·2H_2O (SB/OA·2H_2O = 1:3) before (black) and after (red) dry hydrolysis. Note that the heating rate and the set temperature of the reactor are 2 °C min^{-1} and 50 °C, respectively.

This means that the water molecules of the OA component in the composite were fully lost by dehydration during the dry hydrolytic dehydrogenation reaction. More importantly, the peak intensities of the B−H stretching (dual peaks at 2250 cm^{-1}) and bending (1120 cm^{-1}) vibrations decreased significantly after the reaction, indicating that large amounts of hydrogen were generated by B−H bond cleavage during the reaction. The asymmetric B−O stretching and bending vibrations in the fingerprint region and the strong peak at 1325 cm^{-1}, assigned to the symmetric B−O stretching vibration, verify that $NaBO_2$ is generated as a product of dry hydrolysis of the composite.[49]

CONCLUSIONS

SB is one of the chemical hydrides most frequently used as a hydrogen source to produce pure hydrogen via either thermolytic or hydrolytic dehydrogenation reaction. However, SB normally requires a temperature of at least 500 °C for thermolysis, which, unfortunately, is incompatible with portable or wearable gadgets, and the hydrolytic dehydrogenation of SB is difficult to control at the resulting reaction speed. The dry hydrolysis of the SB/OA·2H_2O composite presented herein requires only a small amount of heat energy equivalent to 50 °C for dehydration of the OA·2H_2O component, and the liberated water molecules subsequently hydrolyze the SB component rapidly to generate pure hydrogen, free of poisonous gas, which can be used as a hydrogen source for lightweight PEMFCs. This means that the dehydration temperature is exactly the same as the hydrolysis temperature; therefore, the onset of the dehydrogenation reaction can be controlled and even tuned by exchanging one hydrate compound with another. Further studies include minimization of the volume expansion of the fuel composite after dry hydrolysis and enabling the reversibility of SB/OA·2H_2O, that is, continuous hydrogenation and dehydrogenation of the fuel composite.

ASSOCIATED CONTENT

Supporting Information

The Supporting Information is available free of charge at https://pubs.acs.org/doi/10.1021/acsomega.1c05571.

Block diagram of the laboratory-designed reactor used in this work for the dry hydrolysis of the SB/OA·2H_2O composite; GC peaks of the air and SB/OA·2H_2O with MS spectra of the air; GC and MS spectra of OA·2H_2O and the SB/OA·2H_2O composite after the dry hydrolysis; and FTIR spectra of SB and OA before and after dry hydrolysis (PDF)

AUTHOR INFORMATION

Corresponding Authors

Joon-Hyung Jin − *Department of Chemical Engineering, Kyonggi University, Suwon-si, Gyeonggi-do 16227, Korea;* orcid.org/0000-0002-8525-0740; Email: jjh1023@kgu.ac.kr

Jihoon Jung − *Department of Chemical Engineering, Kyonggi University, Suwon-si, Gyeonggi-do 16227, Korea;* orcid.org/0000-0001-7370-076X; Email: jhjung@kgu.ac.kr

Authors

Seunghun Shin − *Department of Chemical Engineering, Kyonggi University, Suwon-si, Gyeonggi-do 16227, Korea*

Yunkyeong Kim − *Department of Chemical Engineering, Kyonggi University, Suwon-si, Gyeonggi-do 16227, Korea*

Complete contact information is available at: https://pubs.acs.org/10.1021/acsomega.1c05571

Notes

The authors declare no competing financial interest.

ACKNOWLEDGMENTS

This work was supported by Kyonggi University Research Grant 2021 and by Basic Science Research Program through

the National Research Foundation of Korea (NRF) funded by the Ministry of Education (2021R1/1A2059854).

REFERENCES

(1) Shakun, J. D.; Clark, P. U.; He, F.; Marcott, S. A.; Mix, A. C.; Liu, Z.; Otto-Bliesner, B.; Schmittner, A.; Bard, E. Global warming preceded by increasing carbon dioxide concentrations during the last deglaciation. *Nature* **2012**, *484*, 49−54.
(2) Inoue, T.; Yamada, K. Technology evaluation of zero-carbon power generation systems in Japan in terms of cost and CO2 emissions. *Int. J. Smart Grid Clean Energy* **2020**, *9*, 659−664.
(3) Soeder, D. J. Fossil Fuels and Climate Change. *Fracking and the Environment*; Springer, 2021, pp 155−185.
(4) Soltani, M.; Moradi Kashkooli, F.; Souri, M.; Rafiei, B.; Jabarifar, M.; Gharali, K.; Nathwani, J. S. Environmental, economic, and social impacts of geothermal energy systems. *Renewable Sustainable Energy Rev.* **2021**, *140*, 110750.
(5) Ahmadi, M. H.; Ghazvini, M.; Sadeghzadeh, M.; Alhuyi Nazari, M.; Kumar, R.; Naeimi, A.; Ming, T. Solar power technology for electricity generation: A critical review. *Energy Sci. Eng.* **2018**, *6*, 340−361.
(6) Barbosa de Alencar, D.; de Mattos Affonso, C.; Limão de Oliveira, R.; Moya Rodríguez, J.; Leite, J.; Reston Filho, J. Different models for forecasting wind power generation: Case study. *Energies* **2017**, *10*, 1976.
(7) Li, K.; Bian, H.; Liu, C.; Zhang, D.; Yang, Y. Comparison of geothermal with solar and wind power generation systems. *Renewable Sustainable Energy Rev.* **2015**, *42*, 1464−1474.
(8) Demirel, Y. *Energy: Production, Conversion, Storage, Conservation, and Coupling*; Springer Science & Business Media, 2012.
(9) Park, J.; Baek, J. Evaluation of the Energy Efficiency of the Air Engine. *Trans. Korean Soc. Automot. Eng.* **2015**, *23*, 494−501.
(10) Abe, J. O.; Popoola, A. P. I.; Ajenifuja, E.; Popoola, O. M. Hydrogen energy, economy and storage: review and recommendation. *Int. J. Hydrogen Energy* **2019**, *44*, 15072−15086.
(11) Edwards, P. P.; Kuznetsov, V. L.; David, W. I. F. Hydrogen energy. *Philos. Trans. R. Soc., A* **2007**, *365*, 1043−1056.
(12) Winter, C.-J. Hydrogen energy—Abundant, efficient, clean: A debate over the energy-system-of-change. *Int. J. Hydrogen Energy* **2009**, *34*, S1−S52.
(13) Zhao, Y.; Mao, Y.; Zhang, W.; Tang, Y.; Wang, P. Reviews on the effects of contaminations and research methodologies for PEMFC. *Int. J. Hydrogen Energy* **2020**, *45*, 23174−23200.
(14) Olabi, A. G.; Wilberforce, T.; Abdelkareem, M. A. Fuel cell application in the automotive industry and future perspective. *Energy* **2021**, *214*, 118955.
(15) Lamb, J. J.; Hillestad, M.; Rytter, E.; Bock, R.; Nordgård, A. S. R.; Lien, K. M.; Burheim, O. S.; Pollet, B. G. Traditional Routes for Hydrogen Production and Carbon Conversion. *Hydrogen, Biomass Bioenergy*; Elsevier, 2020; pp 21−53.
(16) Li, S.; Kang, Q.; Baeyens, J.; Zhang, H. L.; Deng, Y. M. Hydrogen Production: State of Technology. *IOP Conference Series: Earth and Environmental Science*; IOP Publishing, 2020; Vol. *544*, p 012011.
(17) Chen, L.; Qi, Z.; Zhang, S.; Su, J.; Somorjai, G. A. Catalytic hydrogen production from methane: A review on recent progress and prospect. *Catalysts* **2020**, *10*, 858.
(18) Siang, T. J.; Roslan, N. A.; Setiabudi, H. D.; Abidin, S. Z.; Nguyen, T. D.; Cheng, C. K.; Jalil, A. A.; Le, M. T.; Sarangi, P. K.; Nanda, S. Recent Advances in Steam Reforming of Glycerol for Syngas Production. *Biorefinery of Alternative Resources: Targeting Green Fuels and Platform Chemicals*, 2020; p 399.
(19) Mohammed-Ibrahim, J.; Moussab, H. Recent advances on hydrogen production through seawater electrolysis. *Mater. Sci. Energy Technol.* **2020**, *3*, 780.
(20) Moradi, R.; Groth, K. M. Hydrogen storage and delivery: Review of the state of the art technologies and risk and reliability analysis. *Int. J. Hydrogen Energy* **2019**, *44*, 12254−12269.
(21) Lang, C.; Jia, Y.; Yao, X. Recent advances in liquid-phase chemical hydrogen storage. *Energy Storage Mater.* **2020**, *26*, 290−312.
(22) Ustolin, F.; Lamb, J. J.; Burheim, O. S.; Pollet, B. G. Energy and Safety of Hydrogen Storage. *Hydrogen, Biomass and Bioenergy*; Elsevier, 2020; pp 133−153.
(23) Hwang, H. T.; Varma, A. Hydrogen storage for fuel cell vehicles. *Curr. Opin. Chem. Eng.* **2014**, *5*, 42−48.
(24) Arat, H. T.; Sürer, M. G.; Gökpinar, S.; Aydin, K. Conceptual design analysis for a lightweight aircraft with a fuel cell hybrid propulsion system. *Energy Sources, Part A* **2020**, *42*, 1−15.
(25) Kim, K.; Kim, T.; Lee, K.; Kwon, S. Fuel cell system with sodium borohydride as hydrogen source for unmanned aerial vehicles. *J. Power Sources* **2011**, *196*, 9069−9075.
(26) Borup, R. L.; Kusoglu, A.; Neyerlin, K. C.; Mukundan, R.; Ahluwalia, R. K.; Cullen, D. A.; More, K. L.; Weber, A. Z.; Myers, D. J. Recent developments in catalyst-related PEM fuel cell durability. *Curr. Opin. Electrochem.* **2020**, *21*, 192−200.
(27) Hamilton, C. W.; Baker, R. T.; Staubitz, A.; Manners, I. B−N compounds for chemical hydrogen storage. *Chem. Soc. Rev.* **2009**, *38*, 279−293.
(28) Jain, I. P.; Jain, P.; Jain, A. Novel hydrogen storage materials: A review of lightweight complex hydrides. *J. Alloys Compd.* **2010**, *503*, 303−339.
(29) Santos, D. M. F.; Sequeira, C. A. C. Sodium borohydride as a fuel for the future. *Renewable Sustainable Energy Rev.* **2011**, *15*, 3980−4001.
(30) Jiang, H.-L.; Singh, S. K.; Yan, J.-M.; Zhang, X.-B.; Xu, Q. Liquid-phase chemical hydrogen storage: catalytic hydrogen generation under ambient conditions. *ChemSusChem* **2010**, *3*, 541−549.
(31) Amendola, S.; Sharp-Goldman, S. L.; Janjua, M. S.; Spencer, N. C.; Kelly, M. T.; Petillo, P. J.; Binder, M. A safe, portable, hydrogen gas generator using aqueous borohydride solution and Ru catalyst. *Int. J. Hydrogen Energy* **2000**, *25*, 969−975.
(32) Martelli, P.; Caputo, R.; Remhof, A.; Mauron, P.; Borgschulte, A.; Züttel, A. Stability and decomposition of $NaBH_4$. *J. Phys. Chem. C* **2010**, *114*, 7173−7177.
(33) Liu, Y.; Reed, D.; Paterakis, C.; Contreras Vasquez, L.; Baricco, M.; Book, D. Study of the decomposition of a $0.62LiBH_4$−$0.38NaBH_4$ mixture. *Int. J. Hydrogen Energy* **2017**, *42*, 22480−22488.
(34) Paskevicius, M.; Ley, M. B.; Sheppard, D. A.; Jensen, T. R.; Buckley, C. E. Eutectic melting in metal borohydrides. *Phys. Chem. Chem. Phys.* **2013**, *15*, 19774−19789.
(35) Mao, J.; Gregory, D. Recent advances in the use of sodium borohydride as a solid state hydrogen store. *Energies* **2015**, *8*, 430−453.
(36) Netskina, O. V.; Tayban, E. S.; Prosvirin, I. P.; Komova, O. V.; Simagina, V. I. Hydrogen storage systems based on solid-state NaBH4/Co composite: Effect of catalyst precursor on hydrogen generation rate. *Renewable Energy* **2020**, *151*, 278−285.
(37) Netskina, O.; Tayban, E.; Ozerova, A.; Komova, O.; Simagina, V. Solid-state NaBH4/Co composite as hydrogen storage material: Effect of the pressing pressure on hydrogen generation rate. *Energies* **2019**, *12*, 1184.
(38) Netskina, O. V.; Pochtar, A. A.; Komova, O. V.; Simagina, V. I. Solid-State NaBH4 Composites as Hydrogen Generation Material: Effect of Thermal Treatment of a Catalyst Precursor on the Hydrogen Generation Rate. *Catalysts* **2020**, *10*, 201.
(39) Grochala, W.; Edwards, P. P. Thermal decomposition of the non-interstitial hydrides for the storage and production of hydrogen. *Chem. Rev.* **2004**, *104*, 1283−1316.
(40) U. S. Department of Energy Hydrogen Program. *Go/No-Go Recommendation for Sodium Borohydride for On-Board Vehicular Hydrogen Storage*. Indep. Rev., 2007; p 150.
(41) Schlesinger, H. I.; Brown, H. C.; Finholt, A. E.; Gilbreath, J. R.; Hoekstra, H. R.; Hyde, E. K. Sodium borohydride, its hydrolysis and its use as a reducing agent and in the generation of hydrogen1. *J. Am. Chem. Soc.* **1953**, *75*, 215−219.
(42) Peng, Y.; Zeng, H.; Shi, Y.; Xu, J.; Xie, L.; Cehn, J.; Zheng, J.; Li, X. Oxalic Acid Promoted Hydrolysis of Sodium Borohydride for

https://doi.org/10.1021/acsomega.1c05571
ACS Omega 2022, 7, 979−986

Transition Metal Free Hydrogen Generation. *J. Wuhan Univ. Technol., Mater. Sci. Ed.* **2020**, *35*, 1011−1015.
(43) Kim, G. J.; Hwang, H. T. Thermal hydrolysis of solid-state sodium borohydride for noncatalytic hydrogen generation. *Chem. Eng. J.* **2021**, *424*, 130445.
(44) Ohkubo, M.; Shigetomo, S.; Ukibe, M.; Fujii, G.; Matsubayashi, N. Superconducting tunnel junction detectors for analytical sciences. *IEEE Trans. Appl. Supercond.* **2014**, *24*, 1−8.
(45) Urgnani, J.; Torres, F. J.; Palumbo, M.; Baricco, M. Hydrogen release from solid state NaBH4. *Int. J. Hydrogen Energy* **2008**, *33*, 3111−3115.
(46) Kalantzopoulos, G. N.; Guzik, M. N.; Deledda, S.; Heyn, R. H.; Muller, J.; Hauback, B. C. Destabilization effect of transition metal fluorides on sodium borohydride. *Phys. Chem. Chem. Phys.* **2014**, *16*, 20483−20491.
(47) Botasini, S.; Méndez, E. On the purity assessment of solid sodium borohydride. *J. Power Sources* **2012**, *197*, 218−223.
(48) Mao, J.; Gu, Q.; Guo, Z.; Liu, H. K. Sodium borohydride hydrazinates: synthesis, crystal structures, and thermal decomposition behavior. *J. Mater. Chem. A* **2015**, *3*, 11269−11276.
(49) Andrieux, J.; Demirci, U. B.; Hannauer, J.; Gervais, C.; Goutaudier, C.; Miele, P. Spontaneous hydrolysis of sodium borohydride in harsh conditions. *Int. J. Hydrogen Energy* **2011**, *36*, 224−233.
(50) Muthuselvi, C.; Arunkumar, A.; Rajaperumal, G. Growth and characterization of oxalic acid doped with tryptophan crystal for antimicrobial activity. *Chim. Sin.* **2016**, *7*, 55−62.

https://doi.org/10.1021/acsomega.1c05571
ACS Omega 2022, 7, 979−986